Available online at www.sciencedirect.com
SCIENCE DIRECT
Acta Materialia 54 (2006) 3863–3870
Acta MATERIALIA
www.actamat-journals.com

Texture transition in Cu thin films: Electron backscatter diffraction vs. X-ray diffraction

Petra Sonnweber-Ribic [a], Patric Gruber [b], Gerhard Dehm [c], Eduard Arzt [a,b,*]

[a] *Max Planck Institute for Metals Research, Heisenbergstraße 3, 70569 Stuttgart, Germany*
[b] *Institute for Physical Metallurgy, University of Stuttgart, Heisenbergstraße 3, 70569 Stuttgart, Germany*
[c] *Department of Material Physics, University of Leoben and Erich Schmid Institute of Materials Science, Austrian Academy of Sciences, Jahnstraße 12, 8700 Leoben, Austria*

Received 7 February 2006; received in revised form 7 March 2006; accepted 8 March 2006
Available online 14 July 2006

Abstract

The microtexture of 0.5–10 μm thick Cu films on polyimide substrates was characterized by automated electron backscatter diffraction (EBSD). The transition from a dominant (1 1 1) to a (1 0 0) fibre texture with increasing film thickness is clearly evident and is in agreement with X-ray diffraction measurements. For interpretation of the texture evolution, a driving force map is constructed which displays the energy balance for interfacial and elastic driving forces using experimental yield stress values. The observations follow the predictions of the texture evolution model of Thompson and Carel [Thompson CV, Carel R. MSF 1996;204–206:83; Thompson CV, Carel R. J Mech Phys Solids 1996;44:657] but add new elements: the texture does not switch abruptly as predicted by energetic considerations, but a broad transition is found. Furthermore, access to the microtexture as well as grain size statistics is given by the EBSD technique, allowing new insight into the details of texture evolution.

Keywords: Copper; Thin films; Texture; EBSD; XRD

1. Introduction

Controlling the texture of materials is a possible route to tailor their properties: as elastic and plastic properties of crystals depend on the crystallographic direction, the preferred orientation of grains influences the mechanical behaviour of a material and thus the performance and reliability of components and devices. This is especially important for thin films where defined textures develop during deposition and annealing treatments. Texture evolution is mediated by grain boundary motion in preferred directions caused by anisotropic driving forces. While the mere reduction of grain boundary energy, as in normal grain growth, does not favour specific grain orientations, the anisotropy of surface and interface energy can supply an orientation-dependent driving force. This often results in a (1 1 1) orientation of face-centred cubic (fcc) metal films, because the (1 1 1) plane has the lowest surface energy. In contrast, the strain energy of an fcc metal film under thermal strain favours (1 0 0) oriented grains, which possess the smallest strain energy density. Whereas the surface/interface energy is independent of film thickness, the strain energy scales with film thickness and depends on the applied strain. Hence different textures are predicted for varying film thicknesses and strains as described in detail by Thompson and Carel [1]. Experiments on polycrystalline Ag films gave indeed a predominance of (1 1 1) orientations for small film thicknesses and low thermal strains, and a strong (1 0 0) texture component for thicker films and high thermal strains [1,2]. The preferred growth of (1 0 0) grains was also observed by various authors in Cu thin films [3–8]. In all of these studies, X-ray diffraction (XRD) measurements were

* Corresponding author. Address: Max Planck Institute for Metals Research, Heisenbergstraße 3, 70569 Stuttgart, Germany.
E-mail address: arzt@mf.mpg.de (E. Arzt).

1359-6454/$30.00
doi:10.1016/j.actamat.2006.03.057

used for texture characterization. Hence, the relative texture change or the dominant texture component were observed without access to microtexture information.

In this study the transition in microtexture was characterized quantitatively for the first time by using electron backscatter diffraction (EBSD) in a scanning electron microscopy (SEM) instrument. Cu films with different thicknesses (0.5–10 μm) were analysed by EBSD and, for comparison, XRD measurements. The systematic use of EBSD measurements provides, apart from texture information with spatial resolution, access to neighbour relationships as well as grain boundary characteristics and grain size distributions. This information can provide important input for texture evolution models.

2. Experimental

Highly pure (99.996 at.%) Cu films were deposited on polyimide substrates using an ultrahigh-vacuum magnetron sputtering system (DCA Instruments). The thickness of the Cu layers was varied from 0.5 to 10 μm. The film deposition was performed at room temperature at a base pressure of 10^{-8} Pa and a deposition rate of 28 nm/min. After deposition the samples were annealed at 330 °C for 2 h without breaking the vacuum to obtain a stable microstructure with predominantly columnar grains. Higher annealing temperatures were not possible due to the limited thermal stability of the polyimide.

The macrotexture of the heat-treated films was examined using XRD while the local orientation distribution was investigated from EBSD measurements in an SEM instrument. $\theta/2\theta$ scans were performed with a Philips X'Pert MRD diffractometer operating in parallel-beam geometry. Cu Kα radiation emerging from a sealed X-ray tube operated at 45 kV and 40 mA was made parallel using an X-ray lens (polycapillary collimator). The diffracted beam passed a parallel plate collimator (0.18° acceptance angle) and a flat graphite analyser before being detected by a proportional counter. Diffraction patterns were recorded in continuous mode. The scans were carried out between 20° and 130° with a step size of 0.04° and a scan time of 2 s/°. Based on the Harris method [9], the strength of the texture can be quantified by direct comparison of the integrated peak intensities of a textured film with those of an untextured powder sample. This normalization takes into account the influences on the measured peak intensities which do not depend on the volume fractions of the different texture components, i.e. the multiplicity, the atomic scattering factor, the Lorentz polarization factor and possible instrumental effects. The resulting strength of the texture gives a relative measure for the volume fraction of grains oriented with specific hkl planes parallel to the film surface.

Pole figure measurements were performed for the Cu (1 1 1) and (2 0 0) reflections using a Euler cradle. The measurement direction (i.e. the direction of the diffraction vector) with respect to the specimen frame of reference is defined by the angles ψ and ϕ, where ψ is the inclination of the diffraction vector with respect to the specimen surface normal and ϕ is the rotation angle around the specimen surface normal. The integrated intensity depended on the sample tilt angel ψ but was independent of the rotation angle ϕ. Thus, it can be concluded that the films exhibited a fibre texture. Pole figure sections (ψ scans) for the (1 1 1) and the (2 0 0) reflections were generated from the intensity of the diffraction lines measured as a function of ψ. These ψ scans were corrected for background, absorption, tilting and instrumental intensity loss, as in Welzel and Leoni [10]. For texture quantification, the measured and corrected ψ scans were fitted with pole figure sections calculated from theoretical, idealized orientation distribution functions.

The EBSD system (HKL, channel 5) used in this study was attached to a Leo 1530-VP SEM instrument equipped with a field emission gun. The measurements were carried out at a working distance of 13 mm and an accelerating voltage of 20 kV. Areas of 10^2–10^4 μm^2 were scanned at step intervals of 0.05–0.4 μm to determine grain orientations, size and shape. The approximate time per scan was in the region of 1 h. Longer scan times were avoided in order to prevent drift problems. EBSD analyses were repeated over 4–15 different regions for each film thickness to obtain reliable and reproducible data.

The number of grains investigated via EBSD varied from 1800 to 3200 for the different film thicknesses. Using the Tango HKL software, the (1 1 1) and (1 0 0) texture components were divided into subsets in order to allow a separate analysis. For grain detection a critical misorientation of 5° was specified and the twin boundaries were ignored. Furthermore, the boarder grains were excluded from the grain size statistics. A grain was allotted to a particular texture component if at least 50% of the grain possessed this particular orientation. This is especially important, as some grains include twins.

3. Results

3.1. Texture analysis

EBSD orientation maps for the Cu films are shown in Fig. 1. Grains marked blue are oriented with the (1 1 1) plane parallel to the surface, grains in red are (1 0 0) oriented and grains labelled green possess a (1 0 1) orientation. In order to achieve sufficient resolution as well as a large measuring area without prolonging the required scan time, the step size was increased from 0.05 to 0.4 μm with increasing film thickness. The maps clearly reveal a change from a preponderance of (1 1 1) oriented grains for the thinnest film to a predominant (1 0 0) texture component for the 10 μm thick film. This change can be described quantitatively by the volume fractions of grains possessing a particular orientation (Table 1; Fig. 2(a)). These volume fractions were calculated from the area fractions of pixels of a particular orientation assuming a columnar

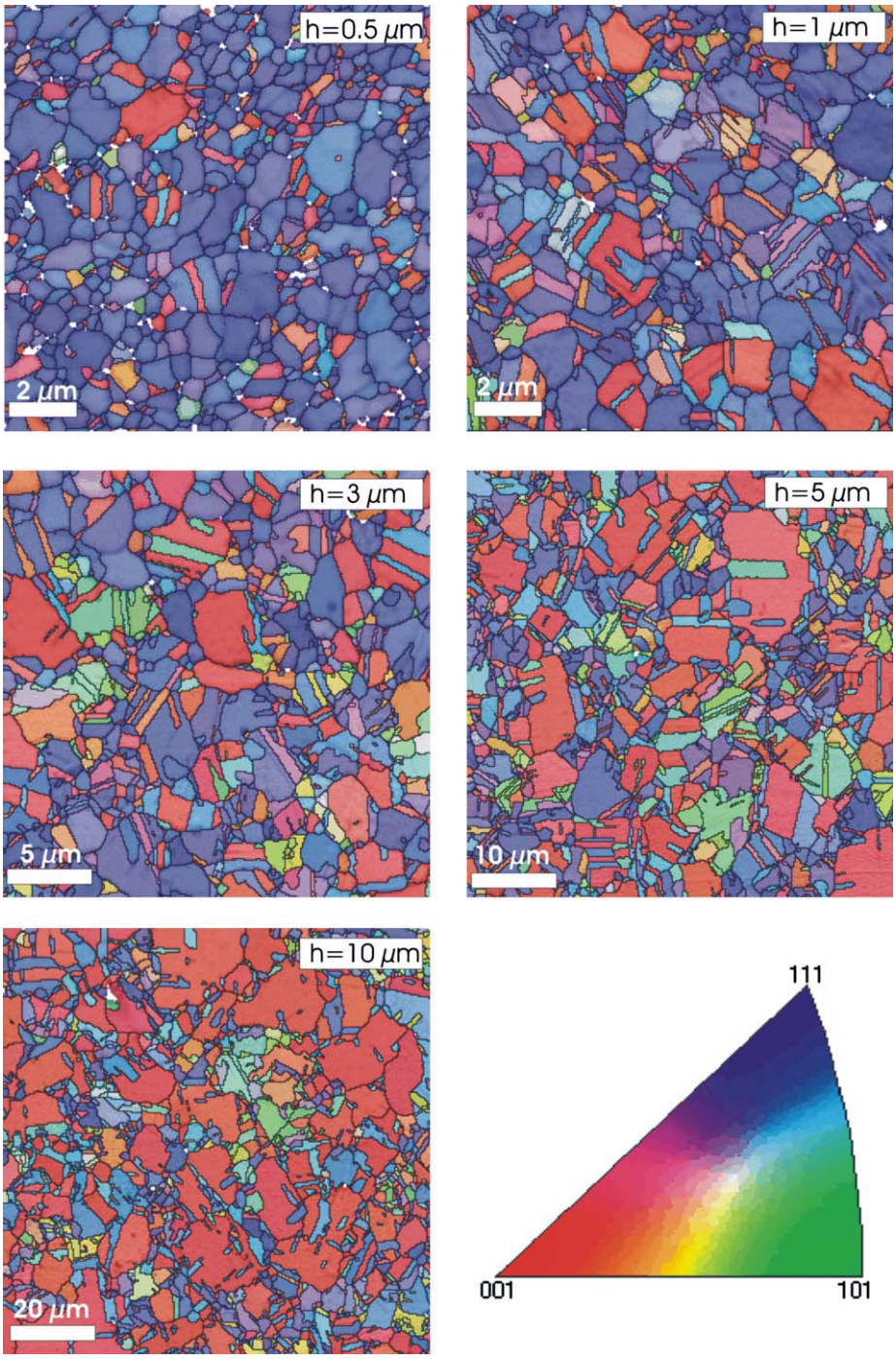

Fig. 1. EBSD orientation maps of Cu films on polyimide with different film thicknesses: 0.5, 1, 3, 5 and 10 μm. The orientation normal to the film surface is represented with the help of the orientation colour key. Note that the scale bar increases from 2 to 20 μm. (For interpretation of the references to colour in this figure legend, the reader is referred to the web version of this article.)

Table 1
Results of EBSD measurements: V_{111} and V_{100} are the volume (area) fractions of (111) and (100) oriented grains

Film thickness (μm)	V_{111} (%)	V_{100} (%)	Total area (μm^2)	Number of specimen sites
0.5	75.9 ± 1.9	10 ± 1.3	1250	8
1	57.7 ± 2.5	19.8 ± 2.8	1250	8
3	44 ± 3.5	27.5 ± 2.8	12,500	8
5	28 ± 4.2	38.8 ± 3.2	10,000	4
10	17.7 ± 0.7	55.9 ± 1.7	40,000	4

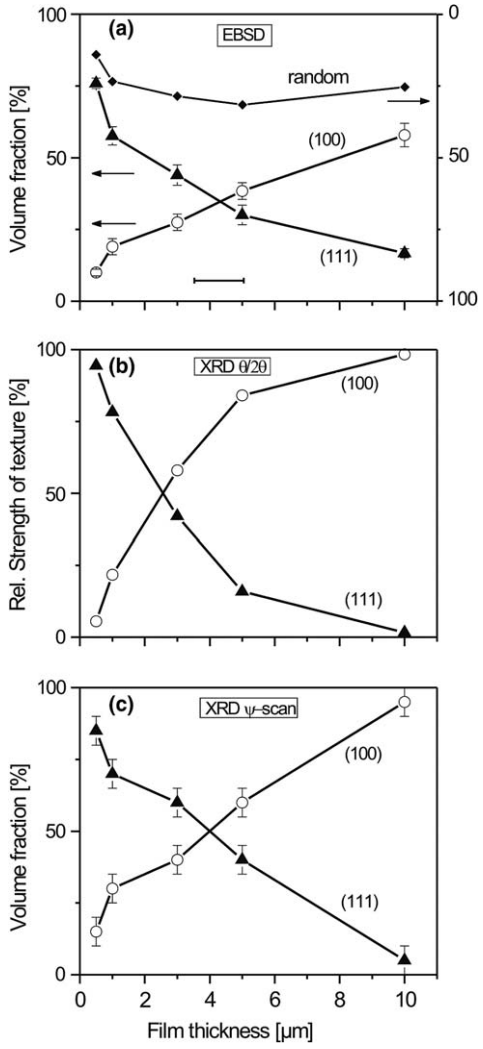

Fig. 2. (a) EBSD results. Volume fraction of (111) and (100) oriented grains as a function of film thickness. A maximum misorientation angle of 15° was allowed for assignment of orientation to each texture component. The random fraction includes all other orientations. The error bars represent the standard deviation of the measurements. If the maximum misorientation angle were changed by ±5%, the crossover would shift by ±0.7 μm (see horizontal bar). (b) $\theta/2\theta$ XRD results. Texture strength as a function of film thickness. The error bar lies within the symbols. (c) Results of ψ scans. Volume fraction of (111) and (100) oriented grains as a function of film thickness. The error is less than 5 vol.%.

microstructure. A maximum misorientation angle of 15° was allowed for assignment of orientations to each texture component. All other grains were classified as "random"; their volume fraction is also displayed in Fig. 2(a). The microtexture of the 500 nm thick film consisted of $75.9 \pm 1.9\%$ (111) and $10.0 \pm 1.3\%$ (100) grains; for the thickest film (10 μm) the fraction of (111) grains decreased to $17.7 \pm 0.7\%$ while the (100) fraction increased to $55.9 \pm 1.7\%$. Between these values, a transition in texture was observed. The interpolated "crossover" occurred at a film thickness of about 4.2 μm. The random fraction increases to a maximum of about 25%.

The XRD $\theta/2\theta$ scans also revealed a predominance of the (111) and (100) texture components, with a negligible (311) peak (less than 2%). In Fig. 2(b), the relative strengths of the (111) and (100) textures are plotted against the film thickness. Again a transition is found, with the crossover now located at a film thickness between 1 and 3 μm. The standard deviation lies in the range of the symbol width. The limitations of this method are discussed in the following section.

Table 2
Results of XRD ψ scans: V_{111} and V_{100} are the volume fractions of (111) and (100) oriented grains (error less than ±5 vol.%), and the sharpness of the distribution is given by the half width w at half maximum

Film thickness (μm)	V_{111} (%)	w_{111} (°)	V_{100} (%)	w_{100} (°)
0.5	85	7	15	32
1	70	8	30	15
3	60	12	40	8
5	40	16	60	10
10	10	25	90	6

The volume fractions resulting from the XRD ψ measurements are shown for the different film thicknesses in Fig. 2(c) and Table 2. Again a crossover in dominant texture is found at a film thickness between 3 and 5 μm. The corresponding texture sharpness, presented by the half width at half maximum of the texture poles, is given in Table 2.

3.2. Grain size distribution

The resulting grain size distributions are shown in Fig. 3. Both the relative and the cumulative frequency (normalized to the total number of (111) and (100) grains) of the (111) and (100) oriented grains are plotted as a function of grain size for the different film thicknesses. Separate analysis shows that the films have roughly a log-normal distribution; their median grain size increases with film thickness (Fig. 4). It is especially noticeable that the median grain sizes for the two texture components agree up to film thickness of 3 μm; above this value, (100) grains show increasingly larger grain sizes. Finally, the relative number of (111) and (100) oriented grains normalized to the total number of grains (including also randomly oriented grains) is shown in Fig. 5.

4. Theoretical considerations for a "driving force map"

The annealing texture of a thin film is controlled by the minimization of its total energy, i.e. grain boundary energy, surface and interface energy and elastic strain energy. Thompson and Carel [1] express the rate of growth of an individual grain as

$$\frac{\mathrm{d}r}{\mathrm{d}t} = M\left[\bar{\gamma}_{\mathrm{gb}}\left(\frac{1}{\bar{r}} - \frac{1}{r}\right) + \Delta W_{\mathrm{s}} + \Delta W_{\varepsilon}\right] \quad (1)$$

where r is the radius of the growing grain and $\bar{r}$ the average grain radius, M is the average grain boundary mobility, $\bar{\gamma}_{\mathrm{gb}}$ is the average grain boundary energy and ΔW_{s} and ΔW_{ε} are the driving forces for surface/interface energy minimi-

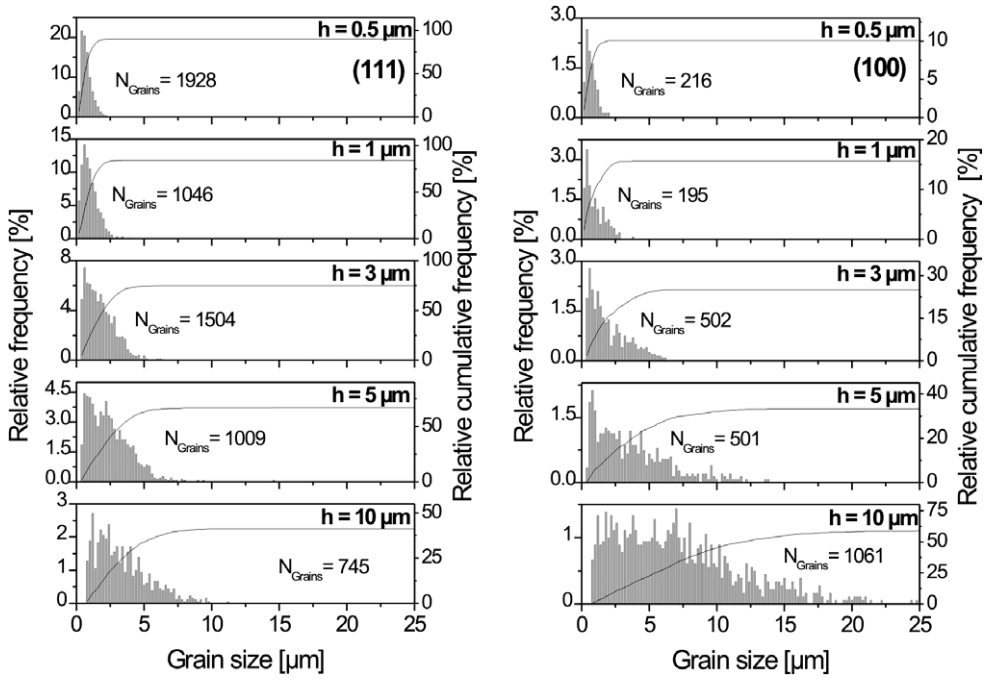

Fig. 3. Grain size histograms and cumulative distributions for (111) and (100) oriented grains. N_{grains}, the number of grains in a particular orientation, was normalized to the sum of (111) and (100) oriented grains.

zation and for strain energy minimization, respectively. The first term results from the reduction of energy by elimination of grain boundaries (normal grain growth). The other two terms are highly anisotropic and can therefore influence the orientation of the growing grain: the favoured texture depends on whether ΔW_s or ΔW_ε dominates [1].

The change in energy ΔW_s caused by the reduction in the average surface energy γ_s and interface energy γ_i of a film is given by [1]

$$\Delta W_s = \frac{\Delta\gamma}{h} \tag{2}$$

where h is the film thickness and

$$\Delta\gamma = \Delta\gamma_s + \Delta\gamma_i \tag{3}$$

with $\Delta\gamma_s$ and $\Delta\gamma_i$ being the differences in the energies of the surfaces and film/substrate interfaces for different grain orientations. Skriver and Rosengaard [11] calculated the surface energies for the different orientations in Cu as 1960 mJ/m^2 for (111) and 2090 mJ/m^2 for (100) grains. There are no values available for the Cu/polyimide interface, and thus the same difference of 130 mJ/m^2 as for the free surfaces was taken for calculations.

The biaxial thermal strain ε in a film on a constraining substrate is given by

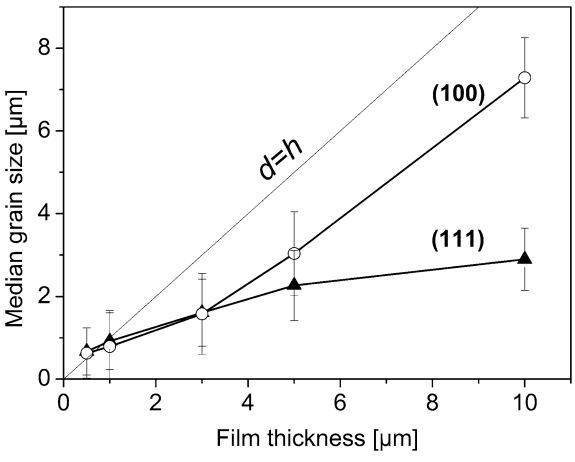

Fig. 4. Median grain sizes for the (111) and (100) texture components as a function of film thickness. The black line corresponds to a simplified stagnation criteria [18].

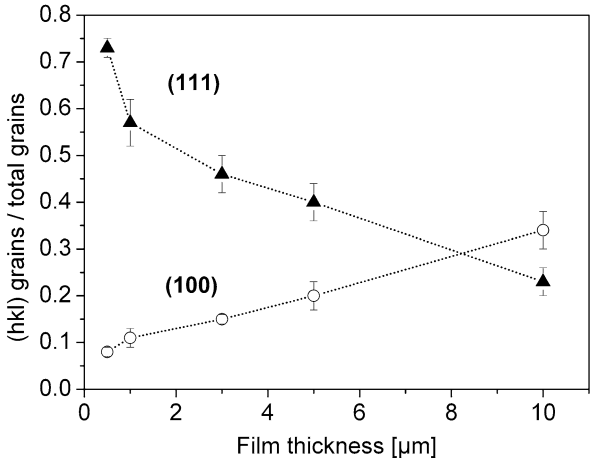

Fig. 5. Number of (111) and (100) oriented grains normalized to the total number of detected grains as a function of film thickness. The error bars represent the standard deviation of the measurements.

$$\varepsilon = \int_{T_{dep}}^{T_a} (\alpha_s - \alpha_f) dT \approx \Delta T(\alpha_s - \alpha_f) \quad (4)$$

where α_s and α_f are the isotropic thermal expansion coefficients of the substrate and the film and T_a and T_{dep} are the annealing and deposition temperature. As all films were deposited nominally at room temperature and annealed at 330 °C, the temperature difference ΔT is 305 K. The thermal expansion coefficients are $\alpha_f = 16.6 \times 10^{-6}$/K for Cu and $\alpha_s = 20 \times 10^{-6}$/K for the polyimide substrate [12].

This thermal biaxial strain results in an orientation-dependent thermal stress and therefore in a texture-dependent strain energy density. If the strain is accommodated elastically, the strain energy density W_ε can be calculated as

$$W_\varepsilon = M_{hkl} \cdot \varepsilon^2 \quad (5)$$

where M_{hkl} is the orientation-dependent biaxial modulus which can be derived from the stiffness tensor of the material. For Cu grains with (100) and (111) orientation, M_{hkl} is isotropic in the plane of the film and is given by $M_{100} = 115$ GPa and $M_{111} = 261$ GPa. Calculating the biaxial moduli for different grain orientations, Zhang et al. [13] found that the four lowest strain energy densities corresponded to grains with (100), (511), (310) and (311) planes oriented parallel to the film plane.

When the yield strength of an orientation is reached, the strain energy density is assumed to saturate at the value

$$W_\varepsilon = \frac{\sigma_{y,hkl}^2}{M_{hkl}} \quad (6)$$

where $\sigma_{y,hkl}$ is the yield strength of the orientation (hkl).

Using Eqs. (4) and (5) for the elastic case, the difference in strain energy density between two neighbouring grains with orientation (111) and (100) is

$$\Delta W_\varepsilon = (M_{111} - M_{100})\varepsilon^2 \text{ (all-elastic case)} \quad (7)$$

This corresponds to the driving force available for grain boundary motion. The driving force increases parabolically with strain (temperature) until the (111) orientation starts to yield. For this case the strain energy density of the (111) grains is constant, but the strain energy density of the (100) orientation can still increase. As a consequence the total driving force is then

$$\Delta W_\varepsilon = \frac{\sigma_{y,111}^2}{M_{111}} - M_{100}\varepsilon^2 \quad (111 \text{ plastic}) \quad (8)$$

This behaviour continues until the (100) oriented grains also start to yield. Then the strain energy difference becomes

$$\Delta W_\varepsilon = \frac{\sigma_{y,111}^2}{M_{111}} - \frac{\sigma_{y,100}^2}{M_{100}} \quad (\text{fully plastic}) \quad (9)$$

For yield stress values we resort to experimental measurements. Hommel and Kraft [14] have determined the yield stress of the (111) and (100) texture component of Cu films on polyimide substrates for film thicknesses between 0.4 and 3.15 μm. Assuming the validity of the Von Blanckenhagen model [15], the experimental yield stress values were fitted by the following $\ln(h)/h$ functions:

$$\sigma_{y,111} = 7.49 \cdot \frac{\ln\left(\frac{h}{2.56\times10^{-10}}\right)}{h} + 164.2 \times 10^6 \quad (10)$$

$$\sigma_{y,100} = 8.55 \cdot \frac{\ln\left(\frac{h}{2.56\times10^{-10}}\right)}{h} + 21.21 \times 10^6 \quad (11)$$

where $\sigma_{y,111}$ and $\sigma_{y,100}$ are given in Pa and h is expressed in m. An equivalent fit would result using the Freund–Nix model [16,17].

Beside these driving forces for grain boundary motion, there exists a stagnation force on the grain boundary motion exerted by thermal grooves. Mullins [18] has calculated this stagnation force as

$$\Delta F_g = \frac{\bar{\gamma}_{gb}^2}{h \cdot \bar{\gamma}_s} \quad (12)$$

where $\bar{\gamma}_S$ is the average surface energy. Following Inman and Tipler [19] a relationship between the surface and grain boundary energy is given by $\bar{\gamma}_{gb} \approx 0.34 \cdot \bar{\gamma}_S$ for Cu. Consequently, Eq. (12) can be written as

$$\Delta F_g \approx \frac{\bar{\gamma}_S}{9h} \quad (13)$$

Assuming the average surface energy to be in the range of 2025 mJ/m^2 (arithmetic mean of the surface energies of (111) and (100) oriented grains), the stagnation force can be calculated.

The result of these calculations can be shown in a "driving force map" (Fig. 6). The black curve (ΔW_s) represents the driving force due to surface/interface energy minimization; it scales inversely with film thickness. The grey curve

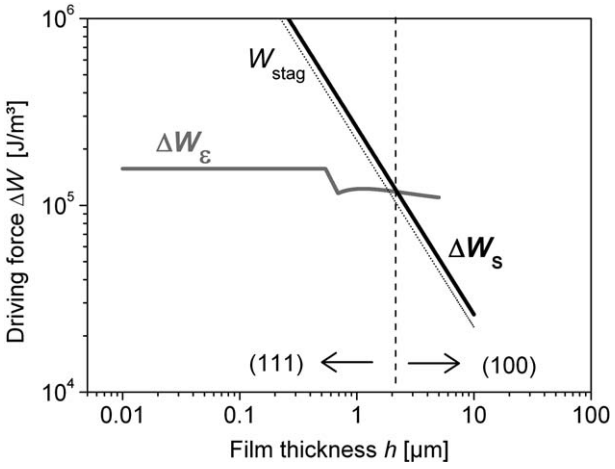

Fig. 6. Driving force map. Estimated driving force for strain energy minimization, ΔW_ε, and surface/interface energy minimization, ΔW_s, for Cu thin films on polyimide. Surface and interface energy minimization (111 texture) dominates below a film thickness of $h = 2.2$ μm while strain energy minimization (100 texture) dominates above this value. The stagnation force due to grain boundary grooves is shown by a black dotted line.

marks the difference in thermal strain energy ΔW_ε between (111) and (100) textured grains for a temperature difference $\Delta T = 305$ K. It is seen that ΔW_ε is constant for small film thicknesses; this is the fully elastic case (Eq. (7)). The end of the elastic regime is reached first for the (111) orientation at a film thickness of 0.5 μm. The elastic driving force then drops according to Eq. (8). At a film thickness of 0.7 μm, the yield stress is also exceeded in the (100) grains and the driving force reaches a lower level (Eq. (9)). In this region (fully plastic), the curve is determined by the difference in yield stresses between the (111) and (100) orientation. The "crossover" in driving forces occurs at a film thickness of about 2.2 μm (dashed vertical line), indicating the energetic preference of the (111) texture for film thicknesses smaller than this critical value and of a (100) texture for larger film thicknesses. Finally, also the stagnation force due to grain boundary grooves is shown in Fig. 6 by a black dotted line; it also scales inversely with film thickness.

5. Discussion

We first direct attention to a comparison of the different analytical methods employed in this study. EBSD is a powerful tool for microtextural analysis: it has the advantage of giving access to all orientations and allows the direct determination of volume fractions. In particular, information about the microstructure is also included in the data. The analysis of the results revealed a broad texture transition from a dominant (111) to a (100) texture with increasing film thickness (Fig. 2(a)). Similar results were obtained from XRD measurements, especially when using ψ scans (Fig. 2(c)): the value for the crossover in the dominant texture is almost identical.

The discrepancy in the total values of volume fractions to the EBSD results, and particularly its increase for thicker films, can most likely be attributed to the role of the random fraction. Whereas the random fraction is explicitly considered in the EBSD analysis, it is neglected in XRD. Okolo et al. [20] demonstrated for Cu films on SiO_2 and Si_3N_4 substrates that pole figure scans do not show unambiguously either the presence or absence of a random fraction; fits of the same quality are possible to ψ scans independent of whether a random fraction is assumed or not. By considering the random fraction (determined by the EBSD measurements in calculating the (111) and (100) volume fraction), excellent agreement between the results of the EBSD and XRD ψ method is reached (Fig. 7). The difference in volume fractions between the two methods lies even within the standard deviation of the XRD ψ results for film thicknesses from 0.5 to 5 μm. On the other hand, it is not possible to reach such an agreement with the $\theta/2\theta$ results. A possible explanation lies in the fact that only planes parallel to the surface are detected and, consequently, these scans are unable to detect an increase in volume fraction due to an increased width of the texture. The width of the (111) texture increases for thicker films (Table 2) while that for the (100) texture decreases; hence the $\theta/2\theta$ method tends to underestimate the (111) volume fraction and to overestimate the (100) fraction for thicker films. Furthermore, the $\theta/2\theta$ scans do not have access to all crystal orientations, e.g. the (511) reflection is not available for these measurements with Cu K_α radiation. Thus, it is difficult to define a possible random fraction. However, the $\theta/2\theta$ scans do provide a quick method for preliminary texture information.

Also the EBSD and the XRD ψ scans have their limitations. The EBSD method is not volume related, as the penetration depth lies in the range of several tens of nanometres. Consequently, the assumption of a columnar grain structure is necessary to obtain the volume fraction of a texture component. And although a predominantly columnar structure was found on cross-sections produced by the focussed ion beam, variations in the grain structure, especially for the thicker films, do occur. Furthermore, the measuring area for EBSD measurements is much smaller than for XRD scans. While EBSD samples an area in the range of 10^2–10^4 μm^2, XRD collects data from an area of several mm^2 and is volume related due to its penetration depth.

One of the main benefits of the EBSD method is that it provides detailed insight into grain size statistics (Figs. 3–5). It is apparent from Fig. 3 that the differences in the grain size distribution between the two texture components increase for larger film thicknesses. Analysis shows that the standard deviations of the near-log-normal distributions are very similar, while the difference in median grain sizes increases for thicker films. Thus, the development of the median grain size (Fig. 4) as well as of grain number (Fig. 5) are texture specific. It is interesting that the median grain sizes for (100) and (111) grains coincide up to a film thickness of about 3 μm; this is at first sight surprising as the (111) orientation is energetically favoured for small thickness. The explanation may lie in the vicinity to the

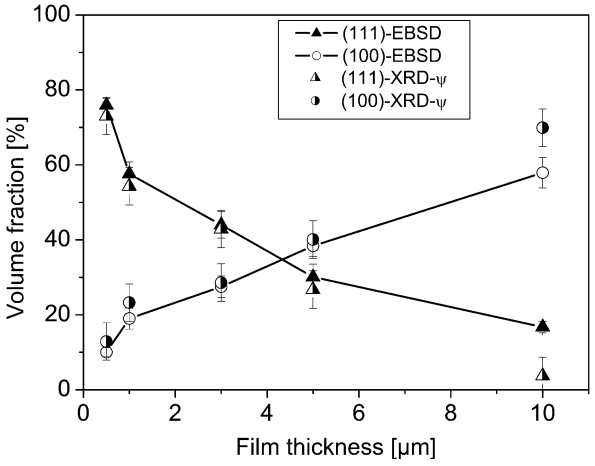

Fig. 7. Comparison of results of EBSD measurements and XRD ψ scans. The random fraction determined by EBSD measurements is considered for the XRD results.

stagnation criterion, drawn as $d = h$ in Fig. 4, which impedes boundary motion even for (1 1 1) grains. Above a film thickness of 3 μm, the median grain sizes diverge. Now the (1 0 0) grains are energetically favoured and grow until they approach the stagnation limit. The unfavourable (1 1 1) grains reach a lower saturation size. The dominance of the (1 1 1) texture in thin films is therefore not due to the larger grain size, but to their much larger number (Fig. 5). In thicker films, the grain numbers seem to converge for the two orientations; the dominance of the (1 0 0) texture can now be attributed to their larger size.

An important observation in Fig. 5 is the fact that the difference in grain numbers between the two texture components is much larger for the thin films than for the thick ones. This behaviour can be explained with reference to Fig. 6: the (1 1 1) component in thinner films has a much larger driving force advantage (of the order of 10^6 J/m^3) than the (1 0 0) component in thinner films (of the order of 10^5 J/m^3). This again confirms the good correspondence between the experimental results and the energetic interpretation.

This also applies to the crossover in driving forces and therefore to the point of texture transition, which is predicted to occur at a film thickness of about 2 μm (Fig. 6). Nevertheless, there is a difference in the experimentally observed texture transition at a film thickness of 4.2 μm. But as the assumed yield stresses enter in a sensitive way (Eq. (9)), a difference of only 20% between (1 1 1) and (1 0 0) oriented grains would cause a shift in the crossover point to 4 μm as observed experimentally. Therefore the agreement between experiment and theory is satisfactory.

A significant observation that cannot be explained by a purely energetic argument is the broad texture transition. The reason for this behaviour must lie in the kinetics of texture evolution which will also depend on the details of the microstructure: grain neighbour interactions or local stagnation conditions can possibly lead to a "sluggish" transition. Such an effect could be accessible by numerical simulation of grain boundary motion, e.g. as in Carel et al. [21].

6. Summary

1. EBSD microtexture measurements of thin Cu films on polyimide substrates revealed a texture transition from (1 1 1) to (1 0 0) at film thicknesses between 3 and 5 μm. Using the EBSD technique, the dominant texture component and the grain size distributions were successfully determined.
2. Detailed comparison with results based on XRD, using both $\theta/2\theta$ and ψ scans, was made. Considering the random fraction accessible only by EBSD measurements, the XRD ψ scan results are in good agreement with EBSD data.
3. The analysis of microtexture by EBSD has provided valuable additional insight. The grain size distributions for the (1 1 1) and (1 0 0) oriented grains show an increasing difference of the median grain size with increasing film thickness. This is explained by the decreasing role of the stagnation force due to grain boundary grooves.
4. In contrast to theoretical predictions, the texture transition is not abrupt; rather, a continuous change from a dominant (1 1 1) to (1 0 0) texture component is observed. The random component increases with film thickness but remains below 25%.
5. The experimental findings can be explained by the texture evolution model of Thompson and Carel [1,2]. A mapping of the driving forces for strain energy and surface/interface energy minimization predicts a texture transition at a similar film thickness as in the experiments.

Acknowledgements

We are grateful to I. Lakemeyer for film deposition and E. Bischoff for an introduction to the EBSD technique. We thank U. Welzel for valuable discussions on the XRD technique and G. Maier, M. Dudek and A. Kumar from the central scientific facility X-ray diffraction for XRD analysis.

References

[1] Thompson CV, Carel R. MSF 1996;204–206:83.
[2] Thompson CV, Carel R. J Mech Phys Solids 1996;44:657.
[3] Zhang JM, Xu KW, Ji V. Appl Surf Sci 2002;187:60.
[4] Zielinski EM, Vinci RP, Bravman JC. J Appl Phys 1994;76:4516.
[5] Zielinski EM, Vinci RP, Bravman JC. Mater Res Soc Symp Proc 1995;391:103.
[6] Harper LME, Gupta J, Smith DA, Chang JW, Holloway KL, Cabral Jr D. Appl Phys Lett 1994;65:177.
[7] Perez-Prado MT, Vlassak JJ. Scripta Mater 2002;47:817.
[8] Perez-Prado MT, Vlassak JJ. MSF 2002;408–412:1639.
[9] Harris GB. Philos Mag 1953;43:113.
[10] Welzel U, Leoni M. J Appl Crystallogr 2002;35:196.
[11] Skriver HL, Rosengaard NM. Phys Rev 1992;B46:7157.
[12] Kapton – polyimide film. Available from: www.dupont.com/kapton/general/sumofprop.html (January 2005).
[13] Zhang JM, Xu KW, Vincent J. Appl Surf Sci 2002;185:177.
[14] Hommel M, Kraft O. Acta Mater 2001;49:3935.
[15] Von Blanckenhagen B. Ph.D. thesis, Department of Physical Metallurgy, University of Stuttgart; 2002.
[16] Freund LB. J Mech Phys Solids 1990;38:657.
[17] Nix WD. Metall Trans A 1989;20A:2217.
[18] Mullins WW. Acta Metall 1958;6:414.
[19] Inman MC, Tipler HR. Metall Rev 1963;8:105.
[20] Okolo B, Lamparter P, Welzel U, Wagner T, Mittemeijer EJ. Thin Solid Films 2005;474:50.
[21] Carel R, Thompson CV, Frost HJ. Acta Mater 1996;44:2479.